MICRO-SCALE EXPERIMENTAL INVESTIGATION OF THE EFFECT OF HYDROSTATIC STRESS ON PORE-SPACE DEFORMATION AND FLUID OCCUPANCY

M. Asadollahkhan Vali[1], A.H. Alizadeh[1], M. Piri[1], and J. Wallace[2]
[1]Department of Petroleum Engineering, University of Wyoming
1000 E. University Ave., Laramie, WY 82071, USA
[2]Hess Corporation, Houston, Texas

This paper was prepared for presentation at the International Symposium of the Society of Core Analysts held in Snowmass, Colorado, USA, 21-26 August 2016

ABSTRACT

Production from hydrocarbon reservoirs increases the effective stress of formation rocks. This results in pore-space deformation, which can impact flow properties, such as absolute and effective permeabilities as well as saturation end points. Previous experimental studies have evaluated the dependence of flow properties on stress at the macro scale; however, no experimental studies have evaluated this effect at the pore scale. In this study, flow experiments were conducted to test the impact of applied stress on permeability, porosity, and saturation profiles on two miniature plug samples of Berea sandstone. A micro-CT scanner was used to capture high-resolution images of the pore structure during core-flooding experiments. Single-phase brine and two-phase oil-brine flow experiments were performed at two levels of isotropic confining pressure. The results showed how the relative movement of the grains due to applied hydrostatic stress altered the rock and flow properties of the core samples, such as porosity, REV, and water saturation, at the micro scale.

INTRODUCTION

Stress variation induces changes in permeability, porosity, elastic moduli, and resistivity [1] and consequently affects the production rate in the life-time of a reservoir [2]. Although variations in single-phase properties, such as absolute permeability, are well investigated at the macro scale [3, 4], the response of multi-phase flow properties to stress variation is not well understood at the micro and macro scales. The lack of appropriate experimental equipment and technology has also led to varying conclusions. Fatt [5] studied gas-oil flow properties at the macro level under stress for the first time. He reported that gas relative permeability characteristics were not affected by overburden pressure. Wilson [6] studied single-phase permeability and two-phase relative permeability under stress conditions and concluded that two-phase relative permeability was less stress sensitive than single-phase permeability. Ali et al. [7] performed a series of experiments on Berea sandstone to measure the reduction in porosity, single-phase permeability, and oil-brine relative permeabilities by increasing overburden up to 6000 psig (radial stress). The results showed increases in initial water saturation and residual

oil saturation as stress was increased. They attributed the increases in irreducible water saturation and residual oil saturation to an increase in capillary forces resulted from the increase in overburden pressure. Al-Quraishi and Khairy [8] reported changes in relative permeability and fluid saturations in multiple stress conditions. They studied the effect of net pressure by decreasing pore pressure at constant confining stress and by increasing confining stress at constant pore pressure. Although their findings confirmed the stress sensitivity of two-phase flow properties, wettability alteration due to injecting crude oil as the aqueous phase arose questions about the results. In the above-mentioned studies, firm conclusions about the effect of stress on single- and two-phase flow properties at the macro scale are lacking.

The advent of X-ray micro-computed tomography has enabled researchers to reach resolutions as low as 2 microns while injecting multiple phases continuously into the micro-scale porous samples [14]. This, therefore, has enabled us to study fluid occupancy and underlying displacement physics at the pore level. Torrealba et al [9] studied the impact of compaction-dependent characteristics of granular packs on fluid flow by performing single- and multiphase flow experiments on bead packs at different confining stress conditions. They reported that porosity, tortuosity, and specific surface area were functions of confining stress as observed in the single-phase flow experiment results. They also reported that, in the two-phase flow experiment, changes in capillary number due to increases in pore velocity during the compaction process had a marginal impact on fluid occupancies in the pore space.

In this study, we utilized X-ray micro-computed tomography techniques with high resolutions to study rock and flow properties during increasing net confining stress. We conducted micro-scale flow tests under single- and two-phase flow conditions to investigate the pore-level displacement physics at different hydrostatic pressure conditions under capillary dominated regimes. For the single-phase flow experiment, the core sample was saturated with brine, and then hydrostatic confining stress was increased. We reported pore-scale observations of single-phase flow to study absolute permeability and porosity reductions due to increases in hydrostatic stress. For the two-phase flow experiment, a brine-saturated core sample was subjected to an oilflood to establish initial water saturation, and then the hydrostatic confining stress was increased to examine two-phase flow properties, such as effective oil permeability and water saturation, and obtain a better understanding of fluid transport under hydrostatic stress conditions.

FLOW EXPERIMENTS

The experiments were conducted at the micro scale under two types of fluid flow conditions: single-phase and unsteady-state two-phase. In both experiments, we used consolidated, high-permeability Berea sandstone core samples to perform the core-flooding experiments and examine the effects of stress on rock and fluid flow properties. To minimize the influence of anisotropy, only the relatively homogeneous cores were selected, and cores with interbedded layers were discarded. In the single-phase experiment, we studied rock and fluid flow properties. Similarly, the two-phase flow experiment was conducted in a sister sample to investigate oil and brine occupancies as

well as effective permeabilities. In order to perform the two-phase flow experiment under capillary dominant regimes, the capillary number for oil injection was maintained below 2.61×10^{-6}. In both experiments, we used micro-CT scanner to obtain high-resolution images of the pore space.

For the single-phase core-flooding experiment, a miniature core sample, 11 mm in length and 5mm in diameter, was cut from a block of Berea sandstone. The aqueous phase was prepared by adding 2 wt% $CaCl_2$ to distilled water. For the two-phase flow experiment, the core sample was cut with a length of 11.53 mm and a diameter of 5 mm. This sample was cut from the same block of Berea sandstone. The petrophysical properties of the of the Berea core samples are shown in Table 1. For the two-phase core-flooding experiment, the aqueous phase was prepared by adding 2 wt% $CaCl_2$ and 7.5 wt% Sodium Iodide to distilled water. The Sodium Iodide was used as an X-ray dopant for the purpose of segmentation of phases in the image analysis process. The concentration level of Sodium Iodide was determined prior to the experiments by performing several two-phase flow tests on sacrificing samples and comparing the quality of the images for segmentation purposes. Physical properties of the fluids used in this study are shown in Table 2. The permeability to brine and the oil effective permeability were determined by measuring pressure drop across the core sample at each flow rate and inserting these data into Darcy's law. The average porosity, pore-size distribution, and water saturation were determined using micro-CT images.

Table 1. Dimensions and petrophysical properties of the of the Berea core samples used for single- and two-phase flow experiments.

Flow experiment	Diameter (mm)	Length (mm)	Φ (from X-ray) (%)	K_{abs} (brine) (mD)
Single-phase	5	11	18.84	652
Two-phase	5	11.53	20.62	790

Table 2. Physical properties of the fluids used in this article. The properties values were measured in the lab under this study.

Fluid	Viscosity (mPa.s)	Density (kg/m^3)	Oil/brine IFT (mN/m)
Brine (single-phase experiment)	1.01	1005	-
Brine (two-phase experiment)	1.05	1012	-
Soltrol 170 (two-phase experiment)	2.6	802.13	37.9

EXPERIMENTAL APPARATUS

The experimental apparatus consists of two main systems, a high resolution micro-CT scanner and a precision core-flooding system designed for small, elongated plugs. Both systems were integrated in such a way that the micro-CT scanner could scan the sample during the core-flooding test without having to remove the sample. The imaging system uses a VERSA-XRM500™ micro-CT scanner manufactured by Xradia. The X-ray source reached to a voltage of 60 kV and a power of 5 W for both experiments. A resolution of 2 µm was attained on the 0.4x objective lens. A closed loop system of Quizix™ pumps, a 700-cm^3 two-phase separator, Rosemount™ differential

pressure transducers, and compensation accumulators were integrated together to perform single- and two-phase flow experiments. Figure 1 shows a detailed schematic diagram of the setup. Hydrostatic confining stress was precisely controlled by one of the dual-cylinder pumps. Two dual-cylinder pumps were assigned to inject fluids through the core at constant-flow-rate mode. Pore pressure was maintained using a dual-cylinder pump (i.e., the back pressure pump), which received the fluid from the core at constant-pressure-mode. The back pressure pump discharged the fluids received from the core sample into the separator. The pressure of separator was compensated by a dual-cylinder pump for positive or negative accumulations. This method provided a reliable phase equilibrium and stable pressure in the separator. More details of the experimental setup can be found elsewhere [11, 12]. The core-flooding setup included a miniature, tri-axial core holder made of carbon fiber to minimize X-ray absorption. A custom-built hydraulic miniature piston at the bottom of the core holder provided axial pressure on the sample. The radial pressure was provided by hydraulic pressure around the sleeve. Both radial and axial pressures were controlled by the pump system.

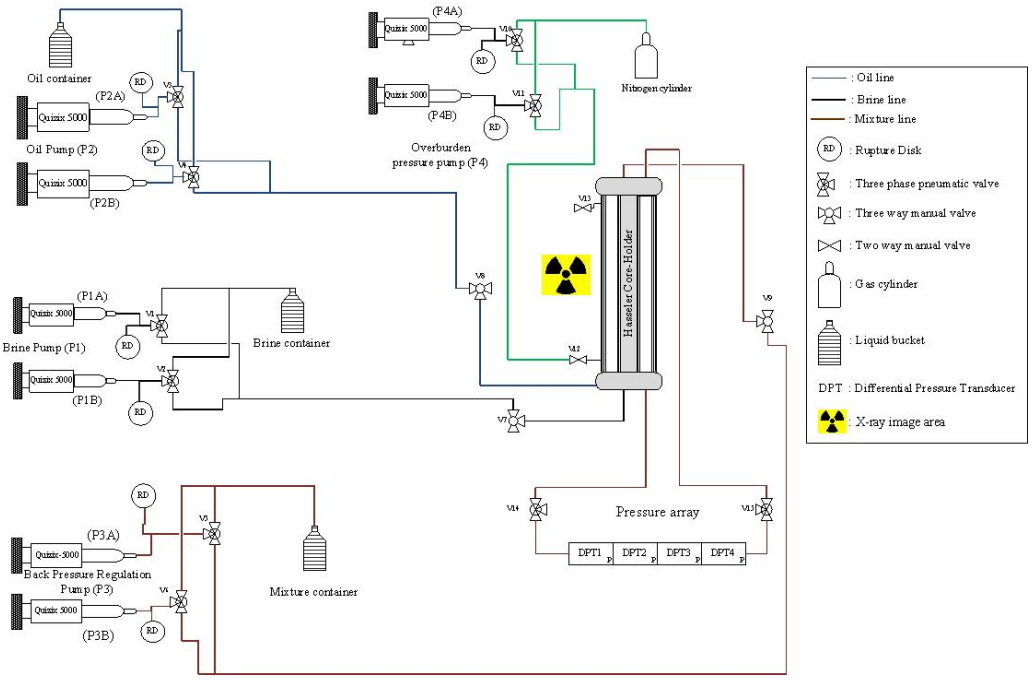

Figure 1. Experimental setup used in this study to perform the core-flooding experiments [11, 12].

EXPERIMENTAL PROCEDURE

The key objective of the study was to assess the effect of stress on single- and two-phase flow properties. During both flow experiments, the confining stress was increased from 600 to 2,000 psig while the pore pressure was maintained at 500 psig. Prior to the experiment, a dry scan was obtained at 100 psig confining stress with atmospheric pore pressure to check the quality of the sample, and then the sample was saturated with brine under 600 psig confining stress and 500 psig pore pressure. The

pressure drop across the core was recorded to measure absolute permeability. The core was re-scanned at 600 psig confining stress, and then confining stress was gradually increased to 2,000 psig in 6 hours while the brine was continuously being injected into the sample. Afterwards, the sample was scanned at 2,000 psig when the pressure drop across the core was stabilized. The two-phase flow experiment was started with a dry reference scan, similar to the single-phase flow experiment, for the quality check at the first step. Then, the sample was saturated with brine under 600 psig hydrostatic confining stress and 500 psig pore pressure. The brine-saturated core was subjected to an oilflood with 0.01 ml/min injection rate (corresponding to a capillary number of 2.61×10^{-6}) to establish initial water saturation. Using this oil flow rate, we reached 55% initial water saturation. The sample was scanned in this step and then the oil flow rate was decreased to 0.001 ml/min. By reducing the oil flow rate, the impact of increasing hydrostatic pressure was only limited to fluid occupancy. After gradually increasing the confining stress to 2,000 psig, pressure data was recorded across the core to ensure that equilibrium was achieved. Then, the same spot was scanned over to investigate pore-scale flow transport.

DATA ACQUISITION, IMAGE PROCESSING, AND ANALYSIS

The image resolution for all experiments was 2 μm, and there was a 4-mm field of view in the middle section of the core. This view provided the best location to measure fluid saturations and other flow properties in both experiments. The initial scan before starting the core-flood took 1 hour, while subsequent main scans took 5 hours. An initial scan was performed at a lower resolution before running the higher resolution scan. The only purpose of performing this short scan was to check the position and initial conditions. Scanning parameters were saved as a recipe in Xradia scanning software. Table 2 shows the scanning parameter for both experiments. The collected tomography files were subsequently reconstructed to create a TXM file as an input for the image analysis software. To determine properties, such as porosity, pore-size distribution, and fluid saturation, AvizoFire™ 9 was used as the image analysis software. The workflow for image analysis consisted of five sections; (i) pre-processing: in this step, several image filters were applied to smoothen the images and remove noises. The best results were produced by applying Non-Local Means filter. Porosity and pore-size distribution can easily be measured after filtering by applying interactive thresholding module; (ii) registration: this step was exclusively performed on two-phase flow images in order to match the two-phase images with the dry reference images and subtract the grains voxel-by-voxel; (iii) arithmetic operations: in order to extract the fluid distribution maps, the pore map was multiplied by the flooded images to obtain a set of images representing the fluid in the pore space; (iv) segmentation: in this step, histogram thresholding method was utilized to segment the two-phases; (v) statistical analysis: in order to quantify statistical properties, such as total saturation and average volume of phases, statistical analysis modules were applied on the segmented images. The above workflow procedure was used before by Alizadeh et al. [13] to segment phases in multiphase flow experiment.

Table 3. Scanning parameters used in both core-flooding experiments.

Voltage	Power	Objective	Exposure time	Resolution
60 kV	5 W	0.4x	5 second	1.98 μm

RESULTS AND DISCUSSION

Increasing confining stress in the single- and two-phase flow experiments induced significant pore-structure deformation resulting in alteration of flow properties. The results of the two experiments are discussed in the following subsections.

A) Single-phase flow experiment

In order to explore deformation of the pore space due to applied stress and study the effects at the micro scale, a single-phase flow experiment was designed and performed. This experiment was conducted at constant pore pressure of 500 psig and under two different hydrostatic confining pressures of 600 and 2,000 psig. After establishing the initial condition (i.e., pore pressure of 500 psig and confining pressure of 600 psig), the confining pressure was gradually increased to 2,000 psig while brine was still being injected at 0.01 ml/min. Figure 2 shows the differential pressure data across the sample as a function of time during the transition step. It was believed that the fluctuations in the recorded data might be due to the pore space deformation after increasing stress as well as slight changes in the lab temperature. As observed, the pressure drop variations reached a plateau after almost seven hours meaning that the applied compaction did not further change the pore space. Changes in the pore space resulted in variations in rock properties (e.g., hydraulic conductivity). By increasing hydrostatic stress on the core sample from 600 to 2,000 psig, absolute permeability to brine dropped from 652 to 407 mD.

In addition to the observed pressure drop variations, direct observations of high-resolution images showed the deformation of the rock structure. Figure 3 depicts an example of pore space deformation as a consequence of applied hydrostatic pressure. The pore element identified by a rectangle in the left image (i.e., at 600 psig hydrostatic pressure) was completely reshaped (see the right image) because of the increase in isotropic stress (600 to 2,000 psig). The response of the pore structure to hydrostatic compaction also manifested itself in the pore-size distribution and consequently in average porosity. The pore-size distribution is plotted at both hydrostatic pressure conditions in Figure 4. As observed, the pore-size distribution shifted to the left meaning that the pore elements were compressed and became smaller as a result of the increase in hydrostatic stress. The gap between two curves on the right side of the plot in Figure 4 indicates that the applied hydrostatic stress had a more significant impact on larger pores. Nevertheless, the deformation was sensed in small pores as well. Average porosity measured at both hydrostatic pressures was consistent with the shift of the pore-size distribution toward smaller elements. The average porosity of the sample dropped from 18.84% at 600 psig to 15.13% at 2,000 psig.

The pore structure deformation may also change the Representative Elementary Volume (REV) of the medium. For a porous medium, a porosity-based REV is defined as the boundary of a region in which measured porosity accurately represents the porosity of

the entire medium [10]. Figure 5 shows the porosity-based REV in both hydrostatic pressure conditions of 600 and 2,000 psig. At both 600 and 2000 psig hydrostatic confining stress, REV was a cube of 1.65mm × 1.65mm × 1.65mm and it did not change after the hydrostatic stress was increased.

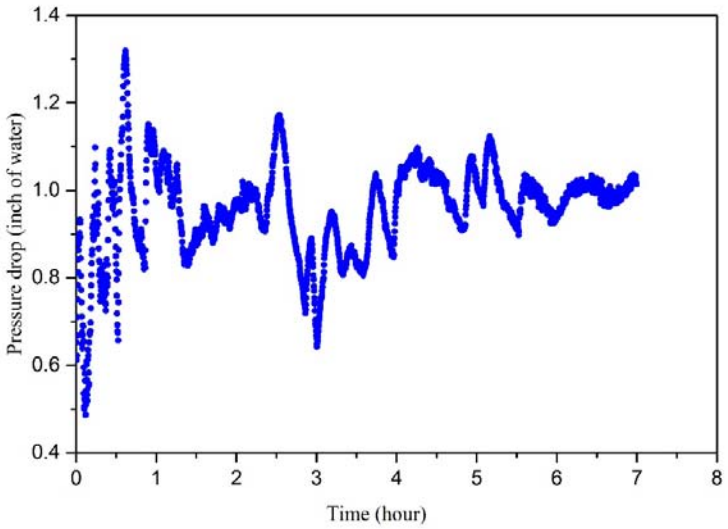

Figure 2. Pressure drop across the core sample as a function of time during the transition step from 600 to 2,000 psig hydrostatic pressure in the single-phase flow experiment.

Our assessments of the effect of hydrostatic compaction on the rock and flow properties during single-phase flow suggested that the reservoir properties, such as porosity and absolute permeability, should continually be modified in reservoir simulators due to variations in stress over the production life of a reservoir in order to improve the performance predications.

B) Two-phase flow experiment

To establish an improved understanding of the effect of stress on multiphase flow at the micro scale, we conducted a two-phase flow experiment at different hydrostatic pressure conditions.

In this flow test, a brine saturated core sample was subjected to an oilflood resulting in an initial water saturation of 55% at 600 psig hydrostatic pressure. Subsequently, the hydrostatic pressure was gradually increased to 2,000 psig to investigate the effect of compaction on two-phase flow properties. The pore structure deformation led to noticeable alterations in effective oil permeability, fluid saturations, and pore-scale fluid configurations. Similar to the single-phase flow experiment, the changes in pressure drop across the core sample indicated the pore structure deformation due to the increase in compaction stress. Figure 6 shows the differential pressure data across the core while injecting oil into the core at a very low flow rate (i.e., 0.001 ml/min). Similar to the findings in the single-phase flow experiment, the increasing pressure drop shown in Figure 6 is an indication of deformation of the pore space after seven hours. During this

period, the applied hydrostatic confining stress deformed the pore space and consequently affected fluid occupancies along the core sample. The initial water saturation of 55% at 600 psig hydrostatic pressure decreased to 50.08% at 2,000 psig. The effective oil permeability was 296 mD at 55% water saturation and at 600 psig hydrostatic confining stress and after hydrostatic pressure was increased to 2,000 psig, it reduced to 169 mD at 50.08% water saturation.

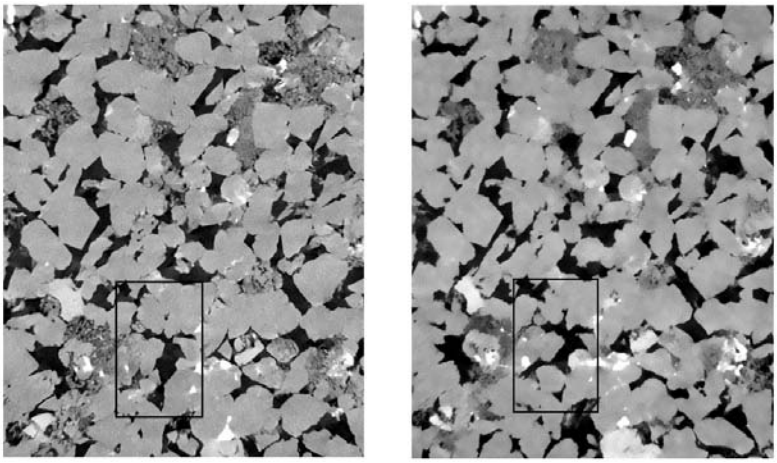

Figure 3. Pore element in the black box at 600 psig hydrostatic pressure (left image) completely reshaped at 2,000 psig hydrostatic pressure (right image).

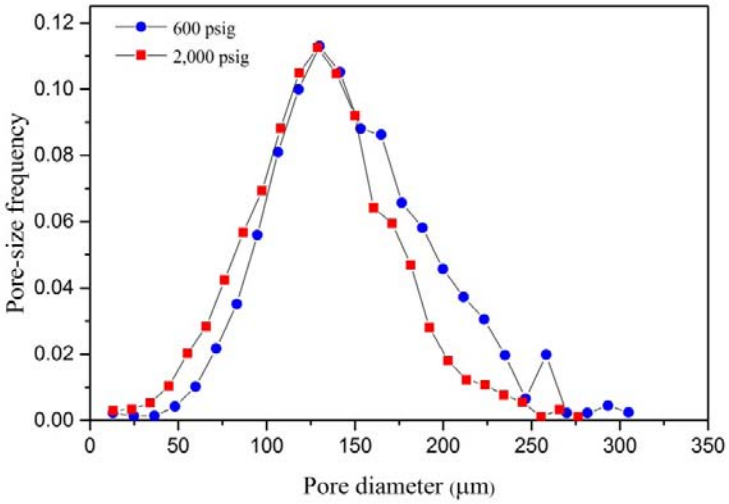

Figure 4. Pore size distributions at 600 and 2,000 psig hydrostatic pressures for the sample used in the single-phase experiment.

During the oilflooding process, oil as the nonwetting phase invades larger pores based on their threshold capillary pressures. However, brine remains in smaller pores and as thin wetting layers in the crevices of the invaded pores. When the hydrostatic pressure is increased and the pore network deforms, the oil may be squeezed out of larger

pore elements and invades neighboring elements. Figure 7 shows an example of this process during which a pore element previously filled with brine at 600 psig hydrostatic confining stress was invaded by oil after increasing the hydrostatic stress to 2,000 psig.

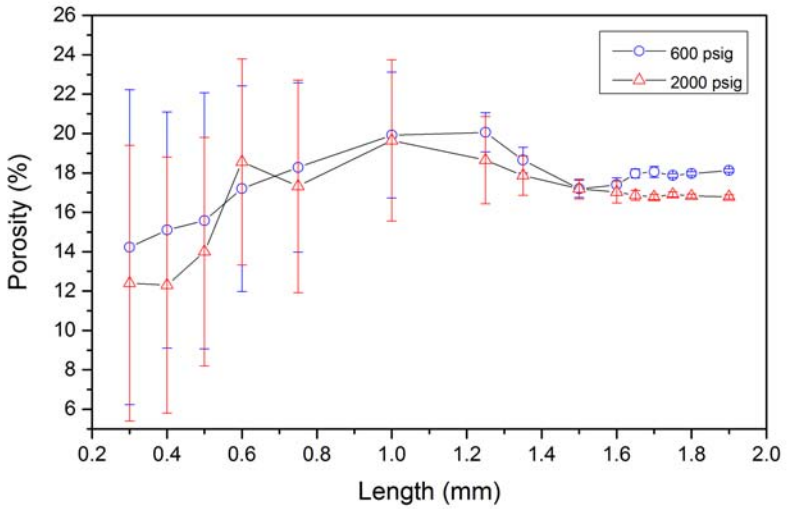

Figure 5. Representative Elementary Volume (REV) of porosity at 600 and 2,000 psig hydrostatic pressures for the sample used in the single-phase experiment. The vertical lines represent error bars.

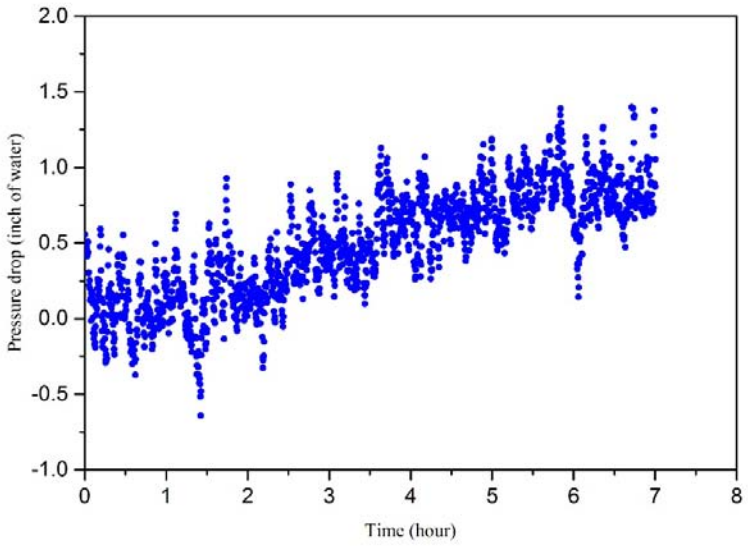

Figure 6. Pressure drop across the core sample as a function of time during the transition from 600 to 2,000 psig hydrostatic pressure in the two-phase flow experiment.

On the other hand, brine in the corners of small elements might have swelled as a result of hydrostatic compaction and displaced or trapped oil. An example of displacing oil with brine is shown in Figure 7 during which a pore element previously filled with oil at 600 psig hydrostatic confining stress was filled with brine after applying 2,000 psig

hydrostatic confining stress. The displacements of brine with oil and oil with brine indicate that the pore network deformation triggers new pore-scale displacements (both oil-to-brine and brine-to-oil). This means that the increase in hydrostatic confining stress provided sufficient changes in local capillary pressure for the displacements to take place.

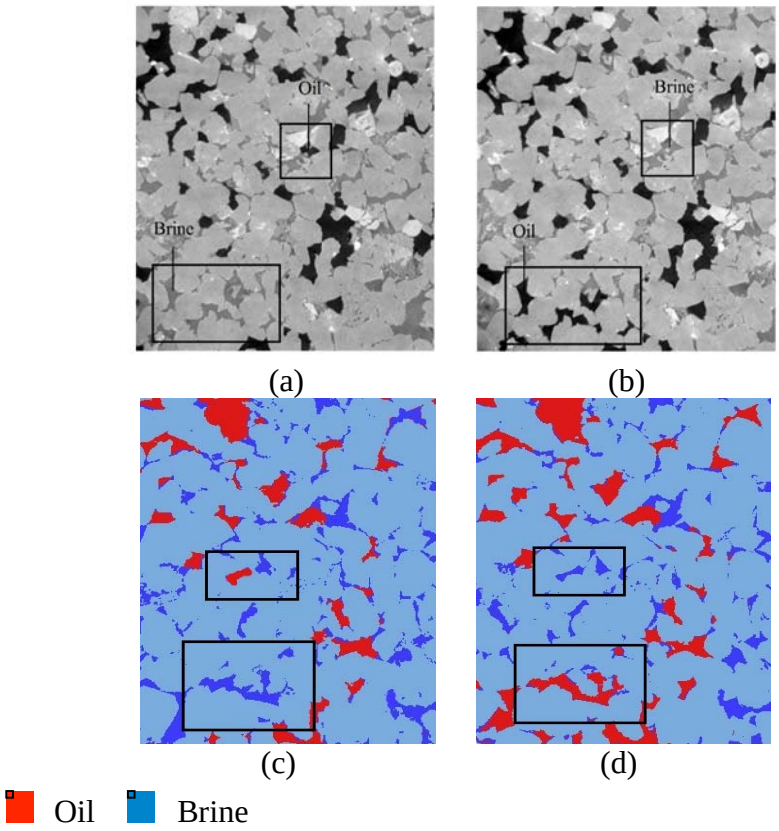

Figure 7. Examples of fluid occupancy of pore elements at 600 psig hydrostatic pressure (left images) compare to that of the same pore elements at 2,000 psig hydrostatic pressure (right images): (a) grey scale image at 600 psig; (b) grey scale image at 2,000 psig; (c) segmented image at 600 psig (red and dark blue indicate oil and brine, respectively); and (d) segmented image at 2,000 psig.

Due to the displacement of brine by oil after increasing the hydrostatic pressure, the connectivity of the oil globules changed as well. Figure 8 shows an example of an oil cluster at 600 psig hydrostatic confining stress (the left image) and the same globule at 2,000 psig hydrostatic pressure (the right image). As observed, the small oil cluster at 600 psig was connected to a much larger oil cluster after the confining stress was increased. It should be noted that although the pore space deformation can change the connectivity of fluid clusters, it does not necessarily mean that increasing hydrostatic pressure will result in better connectivity of fluid clusters.

As observed above, the results of the two-phase flow experiment under different hydrostatic pressure conditions demonstrated the stress sensitivity of fluid occupancies, effective oil permeability, and oil globule connectivity. Therefore, due to the variation of confining stress during the production life of a reservoir, the stress sensitivity of

multiphase flow properties should be considered in reservoir simulations to predict the reservoir flow behavior more accurately.

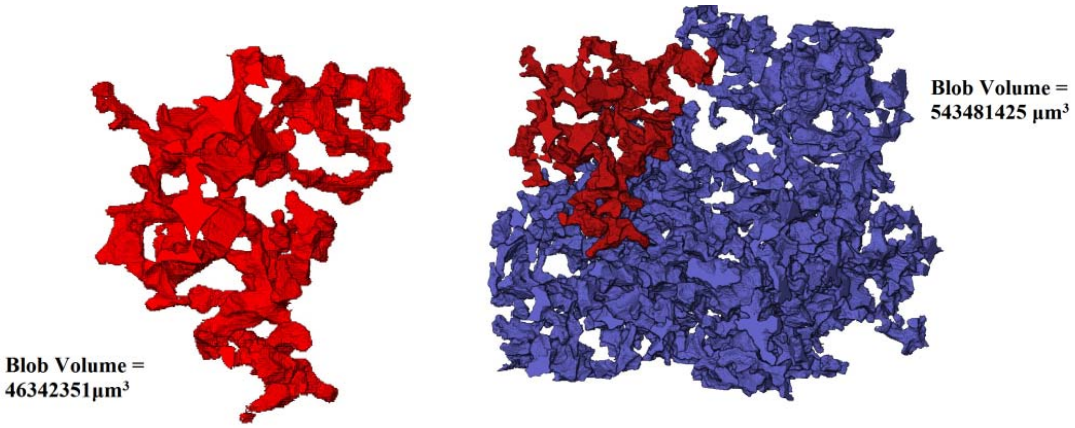

Figure 8. An isolated oil globule at 600 psig hydrostatic confining stress (left image) was connected to a larger oil globule after increasing hydrostatic pressure to 2,000 psig (right image).

CONCLUSIONS

Investigation of the effect of hydrostatic confining stress on rock and flow properties at the pore scale is a need to develop a better understanding of reservoir flow behavior under stress conditions. In this study, the sensitivity of the rock and flow properties to different hydrostatic confining pressures were investigated under the single- and two-phase flow conditions. Below, we summarize the conclusions:

- During the single-phase flow experiment, absolute permeability and average porosity of the medium decreased by increasing hydrostatic pressure. This was caused due to the deformation of the pore space.
- Comparison of the pore size distributions generated under low and high stress conditions indicated that changes in larger pores were greater than those in smaller elements. This explains the significant reduction in porosity.
- The pressure drop data during the transition from 600 to 2,000 psig hydrostatic pressure indicated that there is a time delay until all locations of the core sample feel the applied stress and reach a new steady-state condition.
- Porosity reduction was in the order of 3 to 4% due to the increase in hydrostatic pressure from 600 to 2,000 psig.
- Initial water saturation decreased with increases in applied confining hydrostatic pressure. High-resolution micro-CT images showed that this was due to changes in pore-scale fluid occupancies.
- The connectivity of oil clusters was altered as a result of pore-space deformation after hydrostatic pressure was increased.

ACKNOWLEDGEMENTS

We gratefully acknowledge financial support of Hess Corporation and the School of Energy Resources at the University of Wyoming.

REFERENCES

1. Jones, C., J.M. Somerville, B.G.D. Smart, O. Kirstetter, S.A. Hamilton and K.P. Edlmann "Permeability prediction using stress sensitive petrophysical properties" *Petroleum Geoscience*, (2001) 7, 2, 211-219.
2. Chin, L.Y., Rajagopal Raghavan and L.K. Thomas "Fully coupled geomechanics and fluid-flow analysis of wells with stress-dependant permeability" *SPE Journal*, (2000), 5, (1), 32-44.
3. Fatt, I., D.H. Davis, "Reduction in permeability with overburden pressure" *Journal of Petroleum Technology*, (1952), p16.
4. Dobrynin, V.M. "Effect of overburden pressure on some properties of sandstones" *SPE Journal*, (1962), p360.
5. Fatt, I. "The effect of overburden pressure on relative permeability" *Journal of the American Institute of Mechanical Engineers, Petroleum transactions*, (1953), 198, 325-326.
6. Wilson, J.W. "Determination of relative permeability under simulated reservoir conditions" *Journal of the American Institute of Chemical Engineers*, (1956), 2, 1, 94-100.
7. Ali, H.S., M.A. Al-Marhoun, S.A. Abu-Khamsin, M.S. Celik, "The effect of overburden pressure on relative permeability" *SPE,* (1987), 15730.
8. Al-Quraishi, A. and M. Khairy. "Pore pressure versus confining stress and their effect on oil–water relative permeability curves" *Journal of Petroleum Science and Engineering*, (2005), 48 120– 126.
9. Torrealba, V. A, Z.T. Karpyn, H. Yoon, K. A. Klise, D. Crandall, "Pore-scale investigation on stress-dependent characteristics of granular packs and the impact of pore deformation on fluid distribution" *Geofluids* (2016) 16, 198–207.
10. Bear, J., *Dynamics of Fluids in Porous Media*, Dover, New York, (2002).
11. Piri M. "Recirculating, constant backpressure core flooding apparatus and method" *US Patent* No. WO 2012/082797 A1; (2012).
12. Alizadeh, A.H. and M. Piri, "The effect of saturation history on three phase relative permeability: An experimental study", *Water Resources Research*, (2014); 50(2):1636–64.
13. Alizadeh, A.H., M. Khishvand, M.A. Ioannidis, M. Piri, "Multi-scale experimental study of carbonated water injection: An effective process for mobilization and recovery of trapped oil", *Fuel* (2014) 132, 219–235.